3D Battle-field Radar Detection Range Modularity Method Research

Gao Ying(1), Wang Zidao(1), Guo Shuxia(2), Ge Fei(1)
(1) School of Marine Science and Technology, Northwestern Polytechnical University, Xi'an 710072, China
(2) Science and Technology on UAV Laboratory, Northwestern Polytechnical University, Xi'an 710065, China

Abstract

In order to enhance the scalability of combat system, this paper constructs a Dynamic Library Link (DLL) of radar detection visualization simulation to strengthen extension capacity of application. The result shows that this system is not only lively, but also as module can efficient add on other combat system, provide a new method for integrating complex battle system, have a great significance on battlefield situation assessment.

Index Terms—Radar System; Real-time Visualization; Mesh Data; 3D modularity

1. Introduction

The primary task of this modularity is to visualize invisible radar detection range, and more important is conveniently add on original system. After summarizing the existing achievement and user feedbacks, we discover that the shortcomings in today's real-time combat system are as follows: A. Combat system is too large and complicated. B. Strong coupling between 3D visualization section and system. C. Low portability. In response to these issues, we propose new 3D visualization modularity applied to radar combat modularity. This modularity is based on implicit link library technology. Then 3D scene and radar detection range are generated by inputting visual message.

2. 3D modularity method

2.1 Theory of 3D modularity

We realizing 3D modularity by utilizing dynamic link library (dll), specified function can be encapsulated in dynamic link library and applied to other program without public source code. The advantages of dynamic link library are: A. Good extensibility. B. Multiple program language universality. C. Save Memory. D. Resource sharing. Two kinds of calling dynamic link library methods are explicit invocation and implicit invocation. Explicit invocation loaded the functions of dll into memory when using function. This calling way save memory and have good flexibility. Flow chart shows in figure1, we can obviously see that implicit calling method is faster and easier accessing than explicit calling.

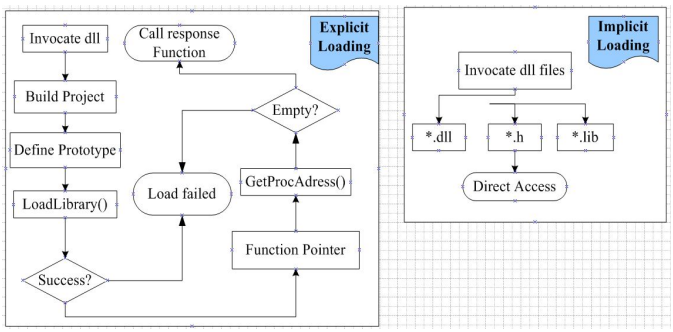

Fig1. Flow chart of load DLL

2.2 Modularity principle framework

This 3D modular include three models: Radar detection range theoretical model, radar jamming model, network data model. The above model is driven by data, by real-time communicating with main system we can obtain those input and output parameters. Framework shows in Figure2.

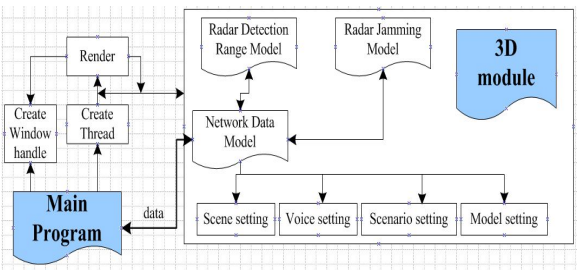

Figure2. 3D visualization module framework

3. Radar detection range theoretical model

2D pattern function is often used in calculating radar detection range. According to antenna theory, 2D pattern function can be deduced from 1D function. As shown in equation (1):

$$F(\theta,\varphi)=k\bullet \mathrm{F}(\theta)\bullet \mathrm{F}(\varphi) \tag{1}$$

Where $\mathrm{F}(\theta)$ and $\mathrm{F}(\varphi)$ are antenna pattern on direction and azimuth, k is maximum antenna gain.

In free space, without considering impact of environment , maximum of the radar detection range is determined by the radar equation, as shown in equation(2):

$$R_{\max}(\theta,\varphi)=\left[\frac{P_t\tau G_r G_t\sigma\lambda^2 F_t^2(\theta,\varphi)F_r^2(\theta,\varphi)}{kT_0B_nF_0D_0(4\pi)^3}\right]^{1/4} \tag{2}$$

Among them, P_t is transmit power of the antenna terminal; τ is pulse bandwidth; G_r is receiving antenna power gain; G_t is transmit antenna power gain; σ is radar target cross-sectional area; λ is wavelength; F_t is factor propagation from transmitting antenna to the target pattern; F_r is propagation factor from targeted to the receiving antenna pattern; k is the Boltzmann constant; T_0 is Standard room temperature; B_n is radar receiver noise bandwidth; F_0 is the noise figure of the receiver; D_0 is radar detection factor. F_t and F_r note When the target is not on the maximum beam direction(G_t and G_r is gain of maximum direction), and the impact of multipath propagation in a non-free-space propagation.

we derived the radar detection range and pattern function theoretical module as shown in equation (3):

$$R(\theta,\varphi)=R_{\max}\times F(\theta,\varphi) \tag{3}$$

According to equation (8), we can obtain the boundary sampling points coordinates in spherical coordinates. Coordinates include longitude, latitude, radius, and then based on spherical Cartesian coordinate conversion formula, we can get the radar border sampling points coordinates in Cartesian coordinates. Finally we connect adjacent sampling points; they will have 3D radar detection range shown as Figure 3.

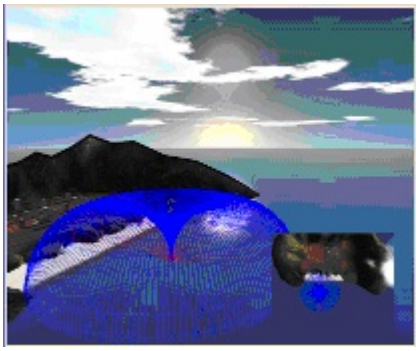

(a)Omni pattern

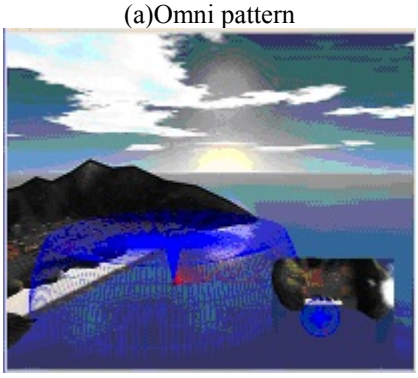

(b) Cosecant squared pattern

Figure3. Radar information based on pattern functions and detection range

4. Radar multiple jamming model

When there are simultaneous multiple interference sources, suppression of jammer on each direction is equivalent to all same direction jam superposition. So we deduce the radar multiple jamming model as shown in equation (4):

$$\sum_{k=1}^{n}\frac{P_{r,k,j}}{P_{r,s}}=\sum_{k=1}^{n}\left(\frac{P_{k,j}G_{k,j}}{P_tG_t}\times\frac{4\pi\gamma_{i,j}}{\sigma}\times\frac{G'_{k,t}}{G_t}\times\frac{R_t^4}{R_{k,j}^2}\right)\geq K_j \tag{4}$$

By equation (4), region boundary equation as shown in equation (5):

$$R_t=\left(K_j\Big/\sum_{k=1}^{n}\left(\frac{P_{k,j}G_{k,j}\gamma_{k,j}}{P_tG_t\sigma}\times\frac{4\pi}{R_{k,j}^2}\times\frac{G'_{k,t}}{G_t}\right)\right)^{1/4} \tag{5}$$

In the equation (6):

$$\begin{cases} G'_t(\theta)=G_t & 0\leq\theta\leq\dfrac{\theta_{0.5}}{2} \\ G'_t(\theta)=k\left(\dfrac{\theta_{0.5}}{\theta}\right)^2G_t & \dfrac{\theta_{0.5}}{2}<\theta<90^\circ \\ G'_t(\theta)=k\left(\dfrac{\theta_{0.5}}{90}\right)^2G_t & \theta\geq 90^\circ \end{cases} \tag{6}$$

$G'_{k,t}$ is an angle variable between the first and the n*th* interference source signal deviates from the direction of the radar antenna. $G'_n(\theta_n)$ as shown in equation (7):

$$
\begin{cases}
G'_{n,t}(\theta_n) = G_t & 0 \le \theta_n \le \dfrac{\theta_{0.5}}{2} \\
G'_{n,t}(\theta_n) = k\left(\dfrac{\theta_{0.5}}{\theta_n}\right)^2 G_t & \dfrac{\theta_{0.5}}{2} < \theta_n < 90^\circ \\
G'_{n,t}(\theta_n) = k\left(\dfrac{\theta_{0.5}}{90}\right)^2 G_t & \theta_n \ge 90^\circ
\end{cases}
\tag{7}
$$

After computing all jammer suppression in one direction, we can achieve the effective radar detection range in that direction.

5. Inter-module data communication

The main data sources come from real-time network transmission, or manually input the information. Due to the complex type, big amount and multi-batch data, the real-time simulation of multiple radars influenced which with multiple interferences is a more difficult problem. By using the network data structure has good qualities in easy design, good relevance and flexible access, multiple radars and interferences data dealing flow chart as shown in Figure4.

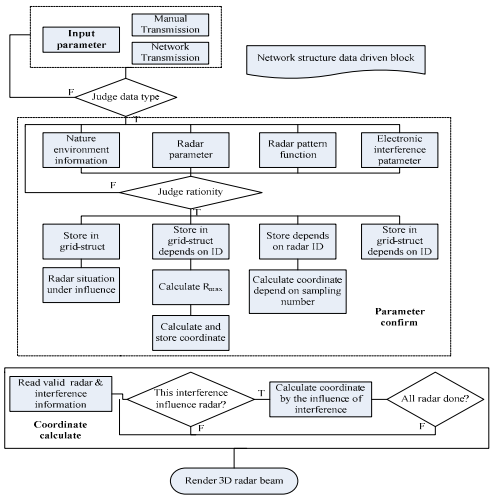

Figure4. Flow chart of Mesh data

The mesh data process include 3 parts of input parameter, parameter confirm and coordinate calculation. Input parameter section involves two ways that include manual and network transmission to obtain parameter. Parameter confirm section aims at distinguish type of input parameters and store them in corresponding structure, afterwards separately calculate the import parameter of each module. The final coordinate calculate section is the key step processing many-to-many radar jamming problem, after calculating all radar jamming circumstance.

6. Results

The software platform of our experiment is based on Qt combining with OpenGL SDK, hardware platform is Intel Core 2 2.8GHz, 2GB RAM, NVIDIA GeForce 9600GT, Windows 7 operation system and radar detection range influenced by dynamic single and multiple interferences experiment as shown in Figure5.

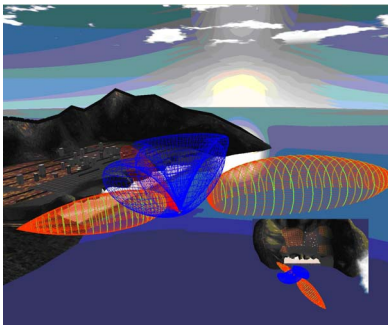

(a) Multiple interference isometric view

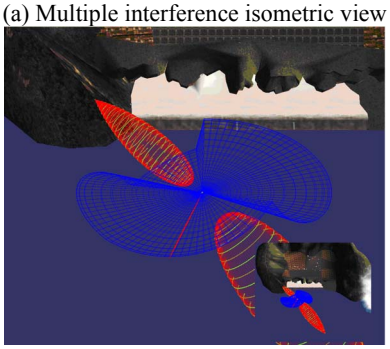

(b) Multiple interference top view

Figure5. Real-time rendering radar detection range influenced by multiple interferences

In Figure5 (a) and (b) shows isometric view and top view, the blue shows the radar beam detection range, and the red beam shows the position and direction of interferences. The red flat face means the radar scanning.

By inputting a large amount of scenario, radar and jammer data, we realize radar combat simulation. Finally we verify 3D modularity by comparing the FPS of module render speed and traditional render speed. The experiment result as shown in Figure 6.

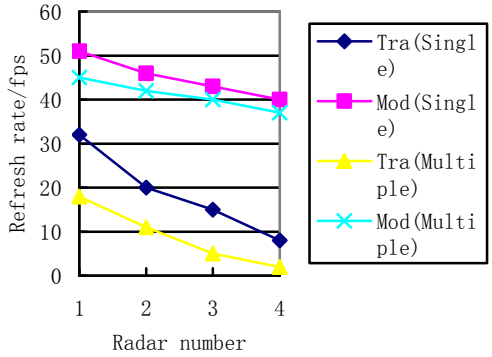

Figure6. Rendering speed of relations between traditional and 3D modular method

After comparing the results of traditional and 3D modular method, we conclude that traditional methods only satisfy circumstance which have few combat platform involved. But when combat platform increasing, differences between traditional and 3D modularity method increasing obvious. This is due to traditional method data store method and calculation processes occupy too much memory, but 3D modularity method simplify radar detection range model, optimize data processing by utilizing network data structure. Encapsulation of input and output optimize the result of calculation, improving FPS by non-uniform sampling method. Advantages gradually became clear with increasing number of platform.

7. Conclusions

Our results confirm the 3D module result which is capable to perform better than traditional method. Moreover they indicate that the performance is dependent on data storage, data processing and number of render point in tasks. Our method can be useful to 3D engineer extending 3D capability on existing systems to perform a visualization task rapidly.

8. Acknowledgements

The authors express sincere gratitude to the other scholars in the field and to all the staff of the project's working group for their support. This project is supported by the National Natural Science Foundation of China, No. 61571368 and China basic research project, No. 07C010.

9. References

1. Zhang J Z, Yuan X J, Zhao X J, “Three-dimensional detection range of radar in complex environment,” *Journal of Computer Applications*, **31**, 10, 2011, pp. 2738-2741.
2. Bartsch M, Clemens M, Hippler T, et al, “Advanced electromagnetic field visualization using the virtual reality modeling language standard,” *IEEE Transactions on Magnetics* (S0018-9464). **37**, 5, 2001, pp. 3604-3607.
3. Su H T, Chan K W, and Snider L A. “Parallel interaction protocol for electromagnetic and electromechanical hybrid simulation.” Generation Transmission and Distribution, *IEEE Proceedings* (S1350-2360), **152**, 3, 2005, pp. 406-414.
4. Antoine Alexandre Journeaux, Frédéric Bouillault, Jean Yves Roger. “Reducing the Cost of Mesh-to-Mesh Data Transfer,” *IEEE Transactions on Magnetics*. *50*, 2, 2014, pp. 701-704.
5. Darren J. Bachmann, Robin J. Evans, Bill Moran, “Game Theoretic Analysis of Adaptive Radar Jamming,” *IEEE Transactions on Aerospace and Electronic systems*. **47**, 2, 2011, pp. 1081-1100.
6. Anatolii Kononov, Kim Jin Ha, Shin Young Cheol, “Noise Jamming Detection Algorithm,” 2013 *IEEE Radar Conference*.
7. Sebastian Grottel, Michael Krone, Christoph Muller, Guido Reina, and Thomas Ertl MegaMol, “A Prototyping Framework for Particle-Based Visualization,” *IEEE Transactions on Visualization and computer graphics*, **21**, 2, 2015, , pp. 201-214.